J Mater Sci (2011) 46:4296–4301
DOI 10.1007/s10853-010-5240-7

IIB 2010

Synthesis of non-equilibrium phases in immiscible metals mechanically mixed by high pressure torsion

Tatsuya Miyazaki · Daisuke Terada · Yoji Miyajima · Challapalli Suryanarayana · Reiko Murao · Yoshihiko Yokoyama · Kazumasa Sugiyama · Minoru Umemoto · Yoshikazu Todaka · Nobuhiro Tsuji

Received: 31 August 2010 / Accepted: 30 December 2010 / Published online: 14 January 2011

Abstract The structural changes in mechanically mixed metals of immiscible combinations of elements caused by bulk mechanical alloying (MA) through the use of high pressure torsion (HPT) were investigated in Ag–Ni and Nb–Zr systems. There was no alloying between Ag and Ni on atomic scale even after 100 rotations of HPT. On the other hand, the β-Zr phase started to appear after HPT 2 rotations in the Nb–Zr system, even though β-Zr is a high temperature phase. Further, Nb and Zr were completely mixed to form a bcc structured single phase after HPT 100 rotations. The sequence of alloying in the Nb–Zr system during HPT was discussed. These results clearly suggest that non-equilibrium phases can form in the Nb–Zr system by bulk MA by the use of HPT.

Introduction

Non-equilibrium phases such as supersaturated solid solutions and amorphous (or glassy) phases are usually synthesized by rapid solidification methods. However, only small pieces, thin films, or ribbons can be produced by these methods because rapid quenching is necessary in order to obtain such non-equilibrium phases through the solidification route. Meanwhile, mechanical alloying (MA) can also produce non-equilibrium phases and alloys of various kinds [1–6]. The technique is most suited for synthesis of alloys from immiscible elements, i.e., those that cannot be alloyed by melting and casting methods [7]. In many cases, MA has been carried out by ball milling of

T. Miyazaki (✉) · D. Terada · N. Tsuji
Department of Materials Science and Engineering, Graduate School of Engineering, Kyoto University, Yoshida Honmachi, Sakyo-ku, Kyoto 606-8501, Japan
e-mail: miyazaki.tatsuya@t05.mbox.media.kyoto-u.ac.jp

D. Terada
e-mail: daisuke.terada@ky7.ecs.kyoto-u.ac.jp

N. Tsuji
e-mail: nobuhiro.tsuji@ky5.ecs.kyoto-u.ac.jp

Y. Miyajima
Department of Materials Science and Engineering, Tokyo Institute of Technology, Nagatsuta-cho, Midori-ku, Yokohama, Kanagawa 226-8503, Japan
e-mail: miyajima.y.ab@m.titech.ac.jp

C. Suryanarayana
Department of Mechanical, Materials and Aerospace Engineering, University of Central Florida, Orlando, FL 32816-2450, USA
e-mail: csuryana@mail.ucf.edu

R. Murao · Y. Yokoyama · K. Sugiyama
Institute for Materials Research, Tohoku University, Sendai 980-8577, Japan
e-mail: r_murao@imr.tohoku.ac.jp

Y. Yokoyama
e-mail: yy@imr.tohoku.ac.jp

K. Sugiyama
e-mail: kazumasa@imr.tohoku.ac.jp

M. Umemoto · Y. Todaka
Department of Production Systems Engineering, Toyohashi University of Technology, Hibarigaoka 1-1, Tempaku, Toyohashi, Aichi 441-8580, Japan
e-mail: umemoto@martens.pse.tut.ac.jp

Y. Todaka
e-mail: todaka@martens.pse.tut.ac.jp

powders. The products obtained by MA are, however, limited to fine powders. Recently, severe plastic deformation (SPD) processes such as accumulative roll bonding (ARB) and high pressure torsion (HPT) have been developed [8, 9]. Although SPD processes are originally used to produce bulk nanostructured metallic materials, they can also be used for MA [10, 11]. MA by the use of SPD processes can produce non-equilibrium phases in bulk shapes. In this study, HPT was used for mechanical mixing of two kinds of elements that are immiscible at room temperature under equilibrium conditions. HPT is a process of imposing torsional strain on the specimen under several GPa of compressive pressure, which can achieve huge equivalent strains. Thus, it is considered possible to synthesize new bulk non-equilibrium phases by MA through the use of HPT.

In this study, Ag–Ni system and Nb–Zr system were selected as the combinations of two immiscible elements. The mixing enthalpy of Ag–Ni system is +15 kJ mol^{-1} [12], which is a relatively large positive value, and that of Nb–Zr system is +4 kJ mol^{-1} [12], which is a relatively small positive value. Both the systems are phase separating type at ambient temperature and pressure according to the phase diagrams shown in Figs. 1 and 2 [13, 14]. The structural changes in mechanically mixed metals of immiscible combinations of elements by bulk MA through the use of HPT have been investigated and the results are reported in this article.

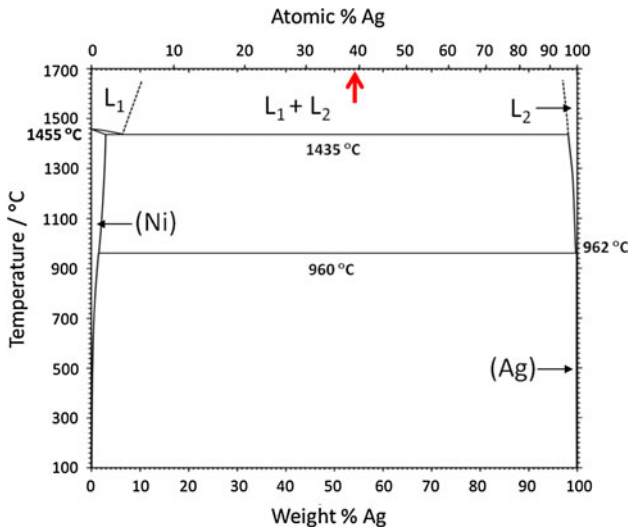

Fig. 1 Phase diagram of Ag–Ni system [13]. The *arrow* attached to the upper horizontal axis indicates the average composition of the Ag–Ni couple used in this study

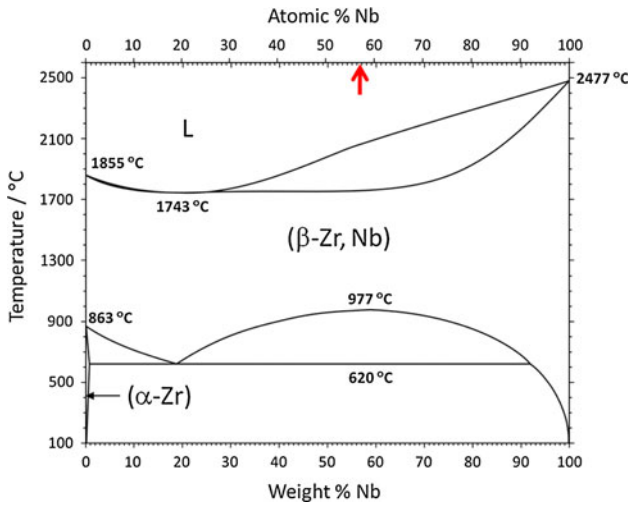

Fig. 2 Phase diagram of Nb–Zr system [14]. The *arrow* attached to the upper horizontal axis indicates the average composition of the Nb–Zr couple used in this study

Experimental procedure

Pure Ag (99.98% purity), pure Ni (99.997% purity), pure Nb (99.9% purity), and pure Zr (99.2% purity) plates with 1 mm thickness were cut into semicircles with 10 mm in diameter using an electric discharge machine. The semicircular plates were then mechanically polished down to 0.65 mm in thickness. In both the systems, a semicircular plate of each of the constituent elements was contacted with one another to be a disk shape. Figure 3 shows the appearance of the specimen for HPT process in the Ag–Ni case. The average compositions of the whole specimens calculated from the volume fraction are indicated by the arrows attached to the upper horizontal axis in Figs. 1 and 2. The specimens were processed by HPT at ambient temperature to different number of rotations $N = 2$, 10, 20, and 100, separately. Figure 4 shows the schematic illustration of the HPT process. During the HPT process, the upper anvil does not move while the lower anvil rotates at a rotation speed of 0.2 rpm, imposing torsional strain on the

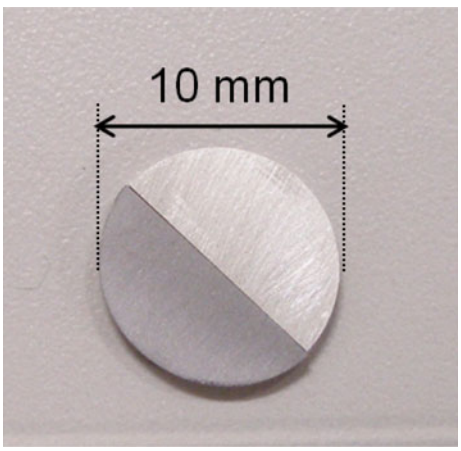

Fig. 3 The appearance of the specimen for HPT process in the Ag–Ni case

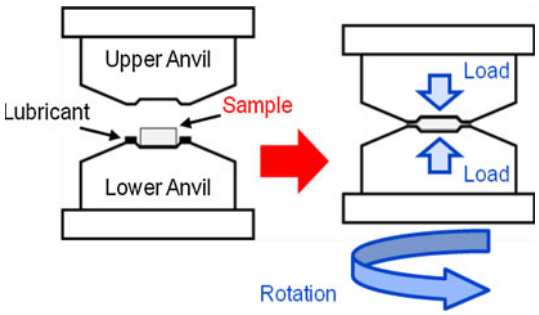

Fig. 4 Schematic illustration of HPT process

specimens under an applied pressure of 5 GPa. The temperature of the specimens during HPT was measured and the increase in temperature was less than 10 K. Therefore, any thermal effects on the specimens can be neglected.

After HPT process, the specimens were cut into two semicircles. Vickers hardness measurements were made with an applied load of 0.98 N for 10 s on the cross-sections of the HPT processed semicircular specimens, as-received materials and specimens that were just compressed at 5 GPa of compressive pressure (as-compressed specimens). X-ray diffraction (XRD) with Cu-Kα radiation was carried out on the HPT processed specimens to identify the phases present. The unit was operated at 45 kV and 40 mA in a scanning step of 0.017°. For XRD analysis the specimens were mechanically polished to obtain flat surfaces. Microstructural observation was conducted on the Nb–Zr specimens after 2 and 100 rotations of HPT by transmission electron microscopy (TEM), and the chemical compositions of the specimens were also analyzed by energy dispersive X-ray spectrometry (EDX). For TEM observation, thin films with about 100 nm in thickness were cut by using focused ion beam (FIB) from the cross-section of the HPT processed semicircular specimens about 3.5 mm away from the center.

Results

Figure 5 shows the Vickers hardness distribution measured on the cross-sections of the Ag–Ni specimens. The Vickers hardness of the as-received Ag and Ni were both about 60 HV, and the hardness values of the as-compressed Ag and Ni were about 80 and 160 HV, respectively. This indicates that strain-hardening in Ni is much larger than that in Ag in the as-compressed specimen. The hardness values of the Ag phase in the HPT processed specimens remained unchanged even though the number of rotations or the distance from the center increased, while those of the Ni phase increased with increasing the distance from the center, and then saturated to the hardness value of about 300 HV. In the $N = 20$ specimen, the hardness values

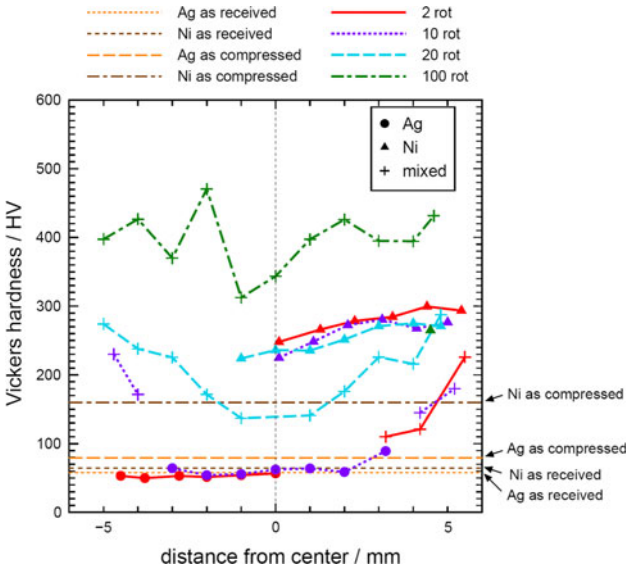

Fig. 5 Vickers hardness distribution of the Ag–Ni specimens

increased as the measured points located farther from the center, but less than those of the Ni phase. On the other hand, the hardness values of the $N = 100$ specimen exceeded the saturation value of Ni at all the measured points.

The Vickers hardness distribution in the Nb–Zr specimens is shown in Fig. 6. The hardness values of the as-received Nb and Zr were about 70 and 190 HV, respectively, and those of the as-compressed specimens reached to about 120 and 200 HV, respectively. The hardness values of both Nb and Zr in the HPT processed specimens increased with increasing the distance from the center, and then reached the saturation values of about 270 HV in Nb

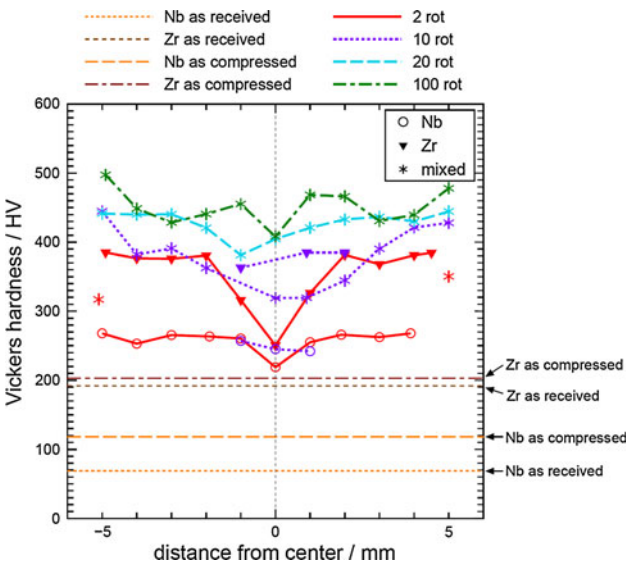

Fig. 6 Vickers hardness distribution of the Nb–Zr specimens

and 390 HV in Zr. However, the hardness values at the fringe of the $N = 10$ specimens exceeded the saturation value of Zr, and the $N = 20$ and 100 specimens also had higher hardness values than the saturation value of Zr along the cross-section of the entire specimen.

Figure 7 shows the XRD profiles of the Ag–Ni specimens deformed by HPT to various rotations. In the Ag–Ni system, peaks of both Ag and Ni were detected in all the HPT processed specimens regardless of the number of rotations, and there was also no change in the positions of the diffraction peaks. This result suggests that Ag and Ni did not form alloys even after HPT 100 rotations.

Figure 8 shows the XRD profiles of the Nb–Zr specimens deformed by HPT to various rotations. In the Nb–Zr system, peaks of bcc-Zr (β-Zr) were detected as well as those of Nb and hcp-Zr (α-Zr) in the $N = 2$ specimen, though it should be emphasized that β-Zr is a high temperature phase in the equilibrium phase diagram (Fig. 2). With increasing numbers of rotations, peaks of α-Zr gradually disappeared, and new peaks began to appear between the peaks of Nb and β-Zr in the $N = 20$ specimen. Eventually, in the $N = 100$ specimen a fully bcc structured single phase was obtained, whose lattice parameter was 0.345 nm. This result indicates that a metastable supersaturated solid solution of Nb and Zr with a bcc structure has formed at room temperature after HPT, even though a mixture of two phases (α-Zr and Nb) is expected to be present under equilibrium conditions. Thus, it can be concluded that non-equilibrium phases have been synthesized in the Nb–Zr system by MA through the use of HPT process.

The microstructure near the Nb/Zr interface in the Nb–Zr $N = 2$ specimen was observed by TEM. Figure 9a

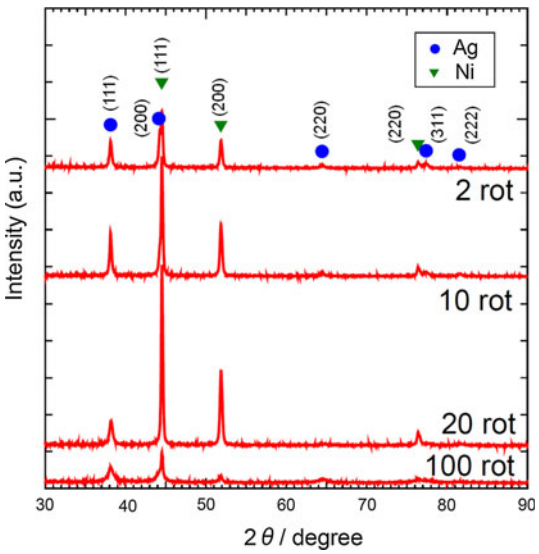

Fig. 7 XRD profiles of the Ag–Ni specimens deformed by HPT to various rotations

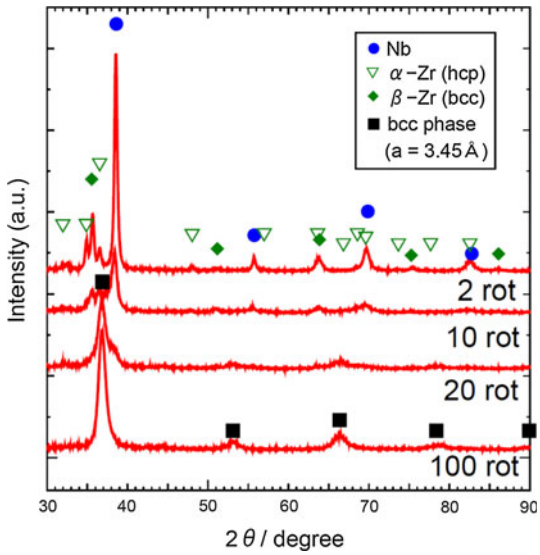

Fig. 8 XRD profiles of the Nb–Zr specimens deformed by HPT to various rotations

shows the bright field image of the observed area, in which the Nb/Zr interface can be easily distinguished because of the remarkable difference between the microstructures of Nb and Zr. Figure 9b shows the selected area electron diffraction (SAED) pattern taken from the Zr area circled in broken lines in Fig. 9a. In Fig. 9b, quarter circles drawn in broken lines at the upper right and lower right of the figure show the diffraction patterns of α-Zr and β-Zr, respectively. Diffraction spots of α-Zr were clearly observed, and in addition to them, those of β-Zr could also be found in the figure. The chemical compositions at the Nb and Zr areas were analyzed by EDX and the results are shown in Table 1. The chemical composition of each area was almost the same as that of the pure metals, which indicates that Nb and Zr were scarcely mixed even near the Nb/Zr interface in the $N = 2$ specimen.

The microstructure of the Nb–Zr $N = 100$ specimens was also observed by TEM. Figure 10a and b show the bright field image and corresponding SAED patterns of the specimen, respectively. Semicircles drawn in broken lines in Fig. 10b indicate the diffraction patterns of the bcc structure. Ultrafine grained structure with grain sizes of less than 100 nm was observed in the area. In Fig. 10b, most of the diffraction spots corresponded to the bcc diffraction rings drawn in the figure. Chemical compositions at three different points indicated in Fig. 10a are shown in Table 2. The points analyzed by EDX were selected from different grains. The result of the chemical composition analysis indicates that Nb and Zr were fully mixed to almost the same atomic fraction at every point. Thus, this ultrafine grained supersaturated solid solution formed by bulk MA through HPT is considered to have homogeneous chemical composition at microscopic level.

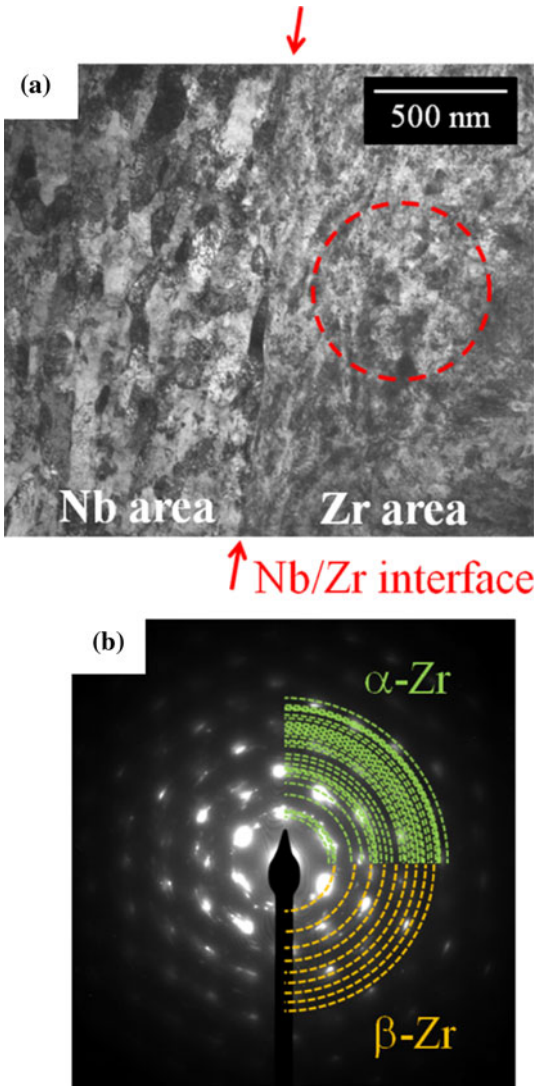

Fig. 9 **a** TEM bright field image near Nb/Zr interface and **b** SAED pattern of the Zr area circled in *broken line* in the $N = 2$ specimen. Quarter *circles* drawn in *broken lines* at the upper right and lower right of the figure show the diffraction patterns of α-Zr and *β*-Zr, respectively

Table 1 Chemical compositions measured by EDX at Nb and Zr areas in the $N = 2$ specimen

Area	(at.%)	
	Nb	Zr
Nb	97.3	2.7
Zr	1.9	98.1

Discussions

In this article, it was clarified that a supersaturated solid solution can be synthesized by bulk MA through HPT process in the Nb–Zr system, which consists of immiscible combination of elements at ambient temperature and

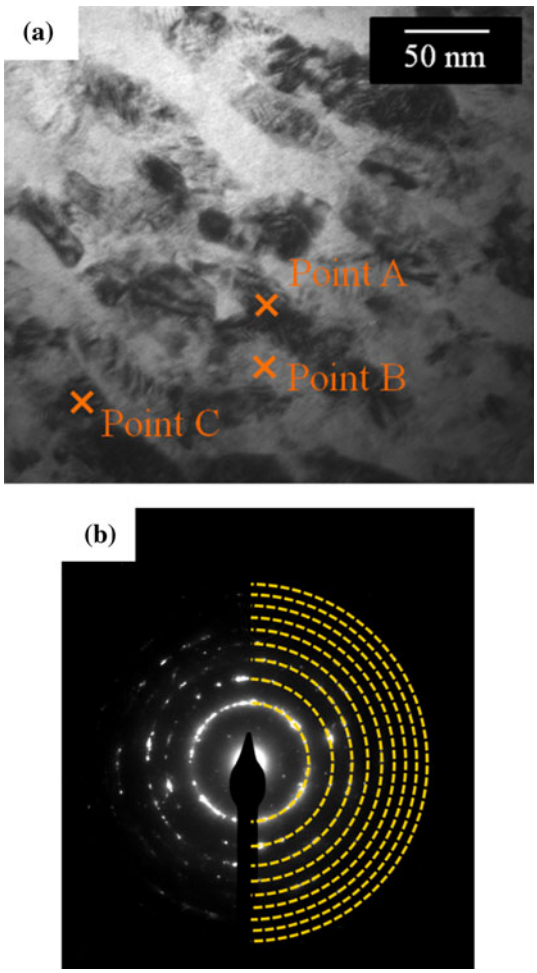

Fig. 10 **a** TEM bright field image and **b** corresponding SAED pattern of the $N = 100$ specimen. *Semicircles* drawn in *broken lines* show the diffraction patterns of bcc structure

Table 2 Chemical compositions measured by EDX at three different points in the $N = 100$ specimen shown in Fig. 10a

Point	(at.%)	
	Nb	Zr
Point A	52.2	47.8
Point B	52.4	47.6
Point C	51.7	48.3

pressure. The bcc structured supersaturated solid solution obtained after 100 rotations of HPT had a lattice parameter of 0.345 nm. Based on the Vegard's law and by the use of the lattice parameters of Nb ($a = 0.330$ nm) and *β*-Zr ($a = 0.357$ nm) [15], the measured lattice parameter of the bcc solid solution should correspond to a chemical composition of $X_{Nb} = 43$ at.% and $X_{Zr} = 57$ at.%. This calculated composition is different from the composition measured by EDX ($X_{Nb} = 52$ at.%, $X_{Zr} = 48$ at.%) or the average composition of the whole specimen ($X_{Nb} = 56$

at.%, $X_{Zr} = 44$ at.%). The lattice parameter of the bcc phase was larger than the expected values calculated from the compositions measured by EDX or the average composition of the whole specimen. This can be attributed to the interaction of Nb atoms and Zr atoms in the Nb–Zr solid solution. Vegard's law assumes ideal solutions which do not have any interaction between the atoms, and considering that Nb–Zr system has a positive heat of mixing, Nb and Zr have some interaction to expand the lattice of the solid solution, making the lattice parameter larger than the calculated value from Vegard's law.

On the other hand, no alloying was recognized in the Ag–Ni system even after HPT 100 rotations. The difference between the Ag–Ni and Nb–Zr systems in the formation ability of alloys may be attributed to the difference in the values of the mixing enthalpy. The mixing enthalpy of the Ag–Ni system is $+15$ kJ mol^{-1}, which is much larger than that of the Nb–Zr system, $+4$ kJ mol^{-1}. There is a possibility that the difficulty in mixing of two kinds of immiscible elements on atomic scale is significantly affected by the value of mixing enthalpy.

The relationship between the formation of β-Zr and progress of mixing of Nb and Zr was investigated by EDX and SAED analysis on the $N = 2$ specimen. From the EDX measurement shown in Table 1, it can be seen that Nb and Zr were scarcely mixed even near the Nb/Zr interface at $N = 2$. On the other hand, diffraction spots of β-Zr could be detected in Fig. 9b which shows the diffraction patterns of the Zr area. Therefore, it is supposed that β-Zr had formed first in α-Zr during HPT process, and then the mixing of Nb and Zr occurred in the bcc phase. It is known that β-Zr can be obtained by applying a large hydrostatic pressure to α-Zr as well as by the application of high temperature [16]. However, the transition pressure is reported to be around 30 GPa, which is extremely higher value than the compressive pressure applied during HPT process in this study. It is reported by Pérez-Prado et al. that β-Zr phase can also be obtained in HPT processed pure Zr [17–19]. Our result supports the previous studies by them, in which the shear induced hcp to bcc transformation in pure Zr by HPT was experimentally observed.

In addition to the structural analysis by XRD and SAED, mechanical properties of the HPT processed specimens were investigated by Vickers hardness measurement. In the Nb–Zr system, the $N = 20$ and 100 specimens and the fringe of the $N = 10$ specimen had higher hardness values than the saturation value of highly strain-hardened Zr. Considering the results of XRD measurement, this hardening can be mainly attributed to the formation of Nb–Zr solid solution. As for the Ag–Ni system, however, the hardness values of the $N = 100$ specimen exceeded the saturation hardness of Ni, though this system did not form any alloys even after 100 rotations of HPT. There can be a possibility that fine lamellar structure composed of nanoscale Ag and Ni layers caused the remarkable hardening of the $N = 100$ specimen.

Conclusions

HPT process was applied as a method of bulk MA to synthesize non-equilibrium phases in immiscible alloy systems. No alloying was noticed in the Ag–Ni system even after HPT 100 rotations. On the other hand, in the Nb–Zr system, β-Zr appeared after HPT 2 rotations, and a fully bcc structured supersaturated solid solution formed after HPT 100 rotations. These results suggest that non-equilibrium phases can be synthesized by bulk MA through the use of HPT.

Acknowledgement This study was financially supported by the Grant-in-Aid for Exploratory Research (contract No. 21656188) as well as that for Innovative Area, "Bulk Nanostructured Metals" (contract No. 2201) through MEXT, Japan.

References

1. Benjamin JS (1976) Sci Am 234:40
2. El-Eskandarany MS, Saida J, Inoue A (2002) Acta Mater 50:2725
3. Liu ZG, Guo JT, Hu ZQ (1995) Mater Sci Eng A 192(193):577
4. Jiang JZ, Gente C, Bormann R (1998) Mater Sci Eng A242:268
5. Suryanarayana C (2001) Prog Mater Sci 46:1
6. Suryanarayana C (2004) Mechanical alloying and milling. Marcel Dekker, New York
7. Ma E (2005) Prog Mater Sci 50:413
8. Saito Y, Utsunomiya H, Tsuji N, Sakai T (1999) Acta Mater 47:579
9. Valiev RZ, Islamgaliev RK, Alexandrov IV (2000) Prog Mater Sci 45:103
10. Sun YF, Todaka Y, Umemoto M, Tsuji N (2008) J Mater Sci 43:7457. doi:10.1007/s10853-008-2634-x
11. Sun YF, Nakamura T, Todaka Y, Umemoto M, Tsuji N (2009) Intermetallics 17:256
12. de Boer FR, Boom R, Mattens WCM, Miedema AR, Niessen AK (1989) Cohesion in metals transition metal alloys. North-Holland Physics Publishing, Amsterdam
13. Singleton M, Nash P (1991). In: Nash P (ed) Phase diagrams of binary nickel alloys. ASM international, Materials Park, OH, pp 1–3
14. Okamoto H (1992) J Phase Equilibria 13(5):577
15. German VN, Bakanova AA, Tarasova LA, Sumulov YuN (1970) Sov Phys Solid State 12:490
16. Xia H, Duclos SJ, Ruoff AL, Vohra YK (1990) Phys Rev Lett 64:204
17. Pérez-Prado MT, Zhilyaev AP (2009) Phys Rev Lett 102:175504
18. Pérez-Prado MT, Sharafutdinov A, Zhilyaev AP (2010) Mater Lett 64:211
19. Zhilyaev AP, Gálvez F, Sharafutdinov A, Pérez-Prado MT (2010) Mater Sci Eng A527:3918